INTEGRATED OPTICAL AND MICROWAVE REMOTE SENSING TO OIL SPILL THICKNESS CLASSIFICATION IN THE GULF OF THAILAND

Teerawat Suwanlertcharoen[1]*, Siam Lawawirojwong[2] and Kampanat Deeudomchan[3]
[1] Geo-Informatics and Space Technology Development Agency (Public Organization), Bangkok 10210, Thailand
Email: teerawat@gistda.or.th

[2] Geo-Informatics and Space Technology Development Agency (Public Organization), Bangkok 10210, Thailand
Email: siam@gistda.or.th

[3] Geo-Informatics and Space Technology Development Agency (Public Organization), Bangkok 10210, Thailand
Email: kampanat.dee@gistda.or.th

KEYWORDS: Oil Spill Thickness, Oil Spill Index, Damping Ratio, Gulf of Thailand

ABSTRACT: Oil spills have significant impacts on the environment, ecosystems, and the economy. It is essential to rapidly monitor the movements of spills and develop comprehensive plans for post-spill management. Satellite remote sensing is a particularly valuable approach for oil spill detection—this technique enables rapid identification of oil spills and can provide crucial information regarding their size, location, extent, and overall coverage on a large scale. The Gulf of Rayong, situated on the eastern coast of Thailand, is a key strategic hub for Thailand's oil and gas exploration and production activities. Unfortunately, this region has experienced numerous oil spills. In this context, this study's primary objectives were to employ the Oil Spill Index (OSI) derived from Sentinel-2B MSI optical imagery, as well as the Damping Ratio (DR), which measures the contrast intensity between VV (vertical transmit and vertical receive) values in clean and slicked seawater, derived from TerraSAR-X and ICEYE X-band microwave images. These methodologies were implemented to detect and classify oil spill thickness, with a specific focus on investigating an oil spill incident that occurred at the Single Point Mooring in the Gulf of Rayong on 25 January 2022. The findings revealed that the OSI obtained from the Sentinel-2B image on 26 January 2022 successfully captured the oil spill incident, allowing the oil thickness to be effectively classified and estimated. This oil code colour and relative thickness values were determined based on the approach adopted by the NOAA's Emergency Response Division. Subsequently, the oil spill's movement and its natural weathering process over time resulted in some oil patches impacting coastal areas. Additionally, the DR calculated from the TerraSAR-X image on 27 January 2022 and the ICEYE X-band image on 30 January 2022 facilitated the detection of remaining oil spills and the identification of areas with varying oil thicknesses. These findings were corroborated by Thaichote imagery and field data and demonstrated that on 30 January 2022, no substantial oil slicks were present, with only sheen layers indicating a thin oil film. Overall, the results of this work highlight the potential of optical and microwave remote sensing as reliable and effective tools for monitoring oil spills and determining oil thickness characteristics.

1. INTRODUCTION

Oil spills have significant impacts, including environmental and ecosystem damage, economic loss, and effects on human health (Laffon et al. 2016). It is essential to rapidly monitor the movements of spills and develop comprehensive plans for managing post-spill incidents. Among the various oil spill detection methods, satellite remote sensing is a particularly valuable approach as this technique enables timely identification of oil spills, providing crucial large-scale information about their size, location, extent, and overall coverage. Using data from multiple microwave and optical images covering an oil spill has proven beneficial for constraining the oil's drift pattern and extent; for example, both optical and microwave time series have previously been investigated (Espeseth et al., 2020). Optical images may detect a combination of the oil's optical properties and those of the sea surface, and the thickness and optical properties of the oil/film will affect the spectral characteristics of the surface, thus resulting in variable spectral signatures (Chatziantoniou et al., 2021). Furthermore, microwave images can identify areas within oil slicks containing relatively thicker or more persistent oil and their short-term drift patterns (Espeseth et al., 2020); in addition, these images are not a ected by cloud cover (Fingas, 2013).

The Gulf of Rayong, situated on the eastern coast of Thailand, is a crucial hub for Thailand's oil and gas exploration and production activities. Massive oil spills occurred in the Gulf of Rayong in 2013 and 2022: on 27 July 2013, a pipeline connecting an offshore oil platform to a tanker at the Single Point Mooring (SPM) caused crude oil to spill into the Sea of Rayong. The resulting oil slick covered an area of approximately 20 km^2 and was estimated to contain around 336–1200 barrels (Ingviya et al., 2020). Recently, on 25 January 2022, an oil spill occurred at the SPM in the same area as in

2013. In this oil spill incident, an estimated total spill volume of more than 140 barrels leaked into the Sea of Rayong and affected the coastal area (Saengtabtim et al., 2022). To assess oil spills such as these, remote sensing can be used. In terms of optical imagery, Sentinel-2 images have previously been used to assess oil spills and classify their thickness using the Oil Spill Index (OSI), which reflects the absorption features of oil and can delineate oil spills (Rajendran et al., 2021a, b; Alabdouli et al., 2023). Furthermore, some studies using microwave images have demonstrated the potential of the Damping Ratio (DR) method to extract oil spills and determine the relative oil thickness within a slick (Skrunes et al., 2017; Skrunes et al., 2019; Espeseth et al., 2020). The DR approach requires only a single polarisation, typically VV (vertical transmit and vertical receive).

To our knowledge, few studies have investigated oil spill thickness classification using a remote sensing approach, especially in the Gulf of Thailand. Here, we focus on two types of optical and microwave remote sensing images to detect remaining oil spills and identify areas characterised by varying oil thicknesses, using a case study of the January 2022 Gulf of Rayong oil spill. The objectives of this study are as follows: (1) employ the OSI derived from Sentinel-2B MSI imagery for optical remote sensing and also the DR derived from TerraSAR-X1 and ICEYE-X8 in X-band imagery for microwave remote sensing to detect and classify the thickness of oil spills and (2) investigate an oil spill incident that occurred at the SPM in the Gulf of Rayong on 25 January 2022.

2. MATERIALS AND METHODS

2.1 Study Area

The study area is located in the Gulf of Rayong, which forms part of the Gulf of Thailand near the Rayong province of Thailand. The study area spans the coordinates 100° 50' E–101° 30' E and 12° 20' N–12° 40' N. (Figure 1). The Gulf of Rayong is an important area for Thailand's oil and gas industry, industrial zones, and ports. Additionally, it serves as a hub for oil and gas exploration and production activities, including the offshore SPM (Figure 1). Furthermore, the neighbouring coastal areas host diverse marine and coastal ecosystems, including seagrass beds and coral reefs.

The northeast and southwest monsoons influence the climate of the Gulf of Thailand. The southwest monsoon originates from the Indian Ocean and brings moisture and rain to Thailand from May to August. The northeast monsoon, which lasts from November to January, brings high pressure that spans the Gulf of Thailand. (Buranaprattheprat, 2008). Based on the 20-year annual wind time series (1997 to 2016), the wind strength in the study area has gradually increased, with the strongest winds originating primarily from the west-southwest (WSW) and northeast (NE). Surface current data indicates a predominant current direction from the west-northwest (WNW) and east-southeast (ESE), with a current speed of around 0–0.4 m/s (Polsomboon and Sriariyawat, 2017; 2022).

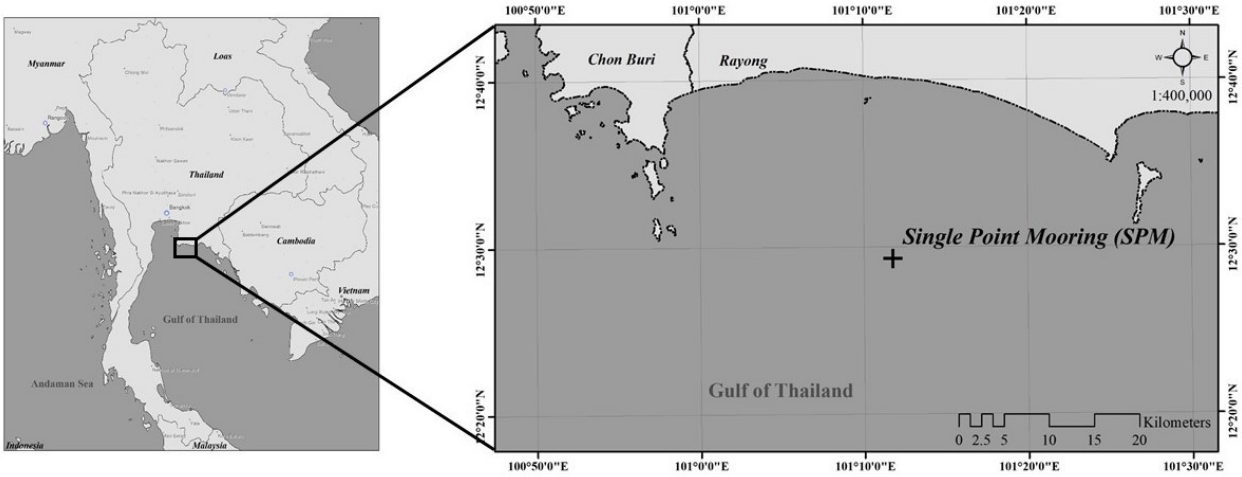

Figure 1. Study area and location of the SPM in the Gulf of Rayong, Thailand

2.2 Data Used

2.2.1 Satellite Imagery

This study used two types of optical and microwave remote sensing data. The optical remote sensing data were derived from two satellites (Sentinel-2B MSI and Thaichote). Level-2A Sentinel-2B MSI imagery with a spatial resolution of 10–60 m from 26 January 2022 was obtained from the Copernicus Open Access Hub (https://scihub.copernicus.eu/dhus/#/home). These data were used to assess the OSI for oil spill detection and thickness classification. In addition, Thaichote images with a spatial resolution of 15 m from 28, 29, and 30 January 2022 were used to verify the oil spill incident, determine the remaining oil spills, and identify areas characterised by varying oil thicknesses. Furthermore, X-band microwave remote sensing images with VV single-polarisation from the oil spill incident were obtained from the Geo-Informatics and Space Technology Development Agency (GISTDA). These include

TerraSAR-X1 data in ScanSAR imaging mode with a spatial resolution of 16 m and ICEYE-X8 data in Stripmap imaging mode with a spatial resolution of 3 m, which were used to calculate the DR for oil spill detection and thickness characterisation. A summary of satellite images used to classify the oil spill thickness during the studied oil spill incident is provided in Table 1.

Table 1. Summary of satellite images used from the oil spill incident

Date	Satellite Image	Time of Acquisition (hh:mm:ss) [UTC+7]
26 January 2022	Sentinel-2B	10:40:19
27 January 2022	TerraSAR-X1	18:23:55
28 January 2022	Thaichote	10:54:40
29 January 2022	Thaichote	10:35:25
30 January 2022	ICEYE-X8	09:57:13
30 January 2022	Thaichote	10:16:27

2.2.2 Ancillary Data

In this study, the ancillary data used include news reports from the area, situation reports from a government agency, and ocean condition data, which were collected and used to evaluate oil spills and their thickness classification during the incident. The ocean condition data from the time of the incident, including surface current and wind data, were used as supporting information to analyse the oil spill's movement and its natural weathering process over time. Wind data were obtained from the closest GISTDA coastal radar station in the study area. The surface ocean currents are derived from Global HYbrid Coordinate Ocean Model (HYCOM) data obtained from NetCDF Subset Service (NCSS) (https://ncss.hycom.org/thredds/ncss/grid/GLBy0.08/expt_93.0/uv3z/dataset.html).

2.3 Methods

The processing steps used in this study are presented in Figure 2. The satellite image pre-processing and image processing steps to detect oil spills and classify their thickness were performed using the Sentinel Application Platform (SNAP) software.

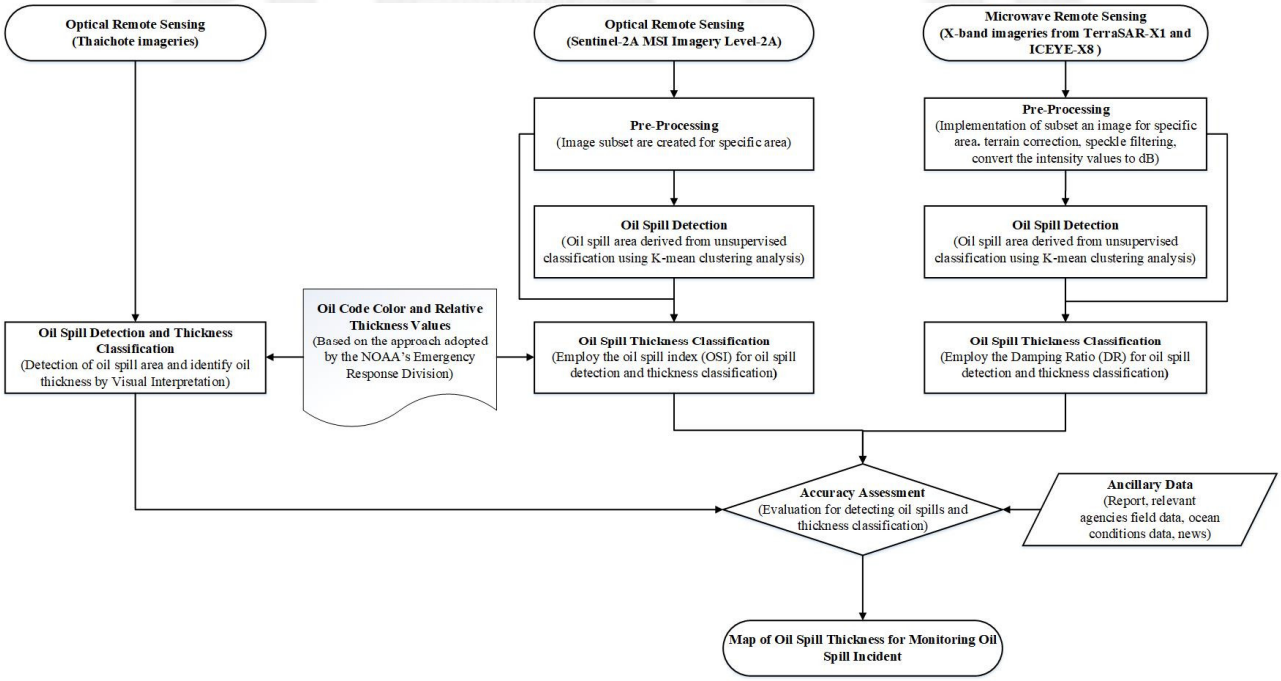

Figure 2. Diagram illustrating the workflow used in this study

2.3.1 Oil Spill Detection

1) Image pre-processing

The pre-processing procedure for the satellite images comprised the following steps: (1) subset optical and microwave satellite images are created for specific areas covering the oil spill incident area, and (2) microwave satellite image processing, which consisted of the following steps: (i) radiometric correction was applied to calibrate the Synthetic Aperture Radar (SAR) for microwave images, (ii) terrain correction was performed using a Range Doppler Terrain

Correction Operator; (iii) speckle filtering was applied to reduce image noise using the Lee speckle filter with a window size of 21 × 21, and (iv) backscattering coefficients (σ) were applied to convert the intensity values to decibels (dB).

2) Image processing

The oil spill detection was performed using the K-means clustering approach. This unsupervised classification method assigns each pixel to the cluster with the closest centre, and the arithmetic mean of all pixels in the cluster is used to calculate the centre. This algorithm's key benefits are its simplicity and speed, which allows it to effectively process large datasets. The results from the K-means clustering analysis were used as oil slick masks for oil spill thickness classification for both optical and microwave imagery and also to classify oil spills into different groups by thickness (only for Sentinel-2B optical imagery).

2.3.2 Oil Spill Thickness Classification

The oil spill thickness classification process employs the OSI derived from Sentinel-2B MSI imagery and the DR derived from TerraSAR-X1 and ICEYE-X8 in X-band imagery to detect oil spills and classify their thickness.

Based on the approach presented by the NOAA's Emergency Response Division in the document titled 'Open Water Oil Identification Job Aid for Aerial Observation' (NOAA, 2016), the oil code colour and relative thickness were used to describe the oil slicks' appearance and classify their thickness based on their visible appearance in optical imagery.

Based on standard observations, the colour and appearance of oil slicks with increasing thickness are as follows: 1) Sheen: a very thin layer of floating oil on the water surface that appears as a silver or rainbow colour; 2) Metallic: the next distinct oil colour, thicker than the sheen (silver and rainbow), tends to re ect the colour of the sky but with some element of the oil colour, typically between a light grey and a dull brown; 3) Transitional Dark: an oil-on-water layer thickness that has typically a transitional dark or oil colour; and 4) Dark, reflecting the continuous true oil colour and representing a layer at least hundreds of micrometres in thickness (NOAA, 2016).

In addition to visual observations, specific spectral indices, such as the OSI, were used to quantitatively measure the detected oil spill extent and determine its thickness characteristics in the marine environment. The OSI and DR indices were calculated as described below.

2.3.2.1 Oil Spill Index (OSI)

The OSI is used to assess oil spills and classify their thickness based on Sentinel-2B imagery. The OSI is calculated as the sum of the green and red wavebands divided by the blue waveband, as below (Rajendran et al., 2021a, b; Alabdouli et al., 2023):

$$OSI = \frac{(Band\ 3 + Band\ 4)}{Band\ 2} \quad (1)$$

where Band 2, Band 3, and Band 4 refer to the surface reflectance value in the blue, green, and red bands of Sentinel-2B imagery, respectively.

2.3.2.2 Damping Ratio (DR)

In this study, the DR was used for oil slick characterisation. Several previous studies have applied the DR to characterise oil slick thickness variations and identify areas containing thicker oil within a slick (Skrunes et al. 2017; Skrunes et al., 2019; Espeseth et al., 2020; Garcia-Pineda et al., 2020). Single-polarisation parameters are used as the DR measures the contrast between VV values in clean and slicked seawater. According to the study by Sergievskaya (2019), the DR tends to increase with increasing oil thickness. The DR for an oil slick is defined as (Skrunes et al., 2019; Brekke and Jones, 2020):

$$DR = \frac{\langle |S_{VV}|^2 \rangle_{sea}}{\langle |S_{VV}|^2 \rangle_{slick}} \quad (2)$$

where $\langle |S_{VV}|^2 \rangle_{sea}$ is the mean intensity of the measured complex scattering for VV polarisation in clean seawater and $\langle |S_{VV}|^2 \rangle_{slick}$ is the mean intensity of the measured complex scattering for VV polarisation in an oil slick area. Typically, the DR is 1 in clean seawater, and in the oil slick area, the DR is > 1.

2.3.3 Evaluation of Oil Spill Detection and Thickness Classification

The detected oil spills and thickness classification were evaluated by comparing the visible appearance of the oil slicks with the oil code colour and relative thickness values based on the approach adopted by the NOAA's Emergency Response Division (NOAA, 2016) for optical remote sensing. In addition, the mapped locations and extents of the area of subsequent oil spill incidents following the oil weathering process were corroborated by RGB true colour composite Thaichote imagery and other relevant data.

3. RESULTS AND DISCUSSION

3.1 Oil Spill Detection and Thickness Classification

On 25 January 2022, an oil spill occurred at the SPM that leaked into the sea. To characterise this incident, we used optical and microwave imagery for oil spill detection and thickness classification, as described below.

3.1.1 Oil Spill on 26 January 2022

The oil slick detected from the Sentinel-2B MSI image acquired on 26 January 2022 at 10:40 UTC+7 was located near the SPM, which was the source of the spill, with a maximum distance from the SPM of around 4.2 km. Based on the K-mean clustering analysis and classification by oil code colour and relative thickness, the oil spill area was found to cover approximately 7.33 km^2 and consisting of Dark (0.25 km^2), Transitional Dark (5.01 km^2), and Metallic (2.07 km^2) classes. Based on the OSI values calculated from Equation (1), zonal statistical analysis for the various classes revealed an average OSI value for Dark oil of 1.18 (±0.14 STD), while Transitional Dark had an average OSI of 0.93 (±0.06 STD), and Metallic had an average OSI of 0.88 (±0.04 STD). The thickness of the oil slick according to the classification type and the OSI values are strongly correlated. The spectral signature analysis results for each wavelength band of the oil slick sample plot area showed that the Dark, where the oil is thickest at the surface area, had the highest surface reflectance in band 4 compared to the Transitional Dark and Metallic classes. In contrast, bands 2 and 3 of the Dark class have lower surface reflectance than the Transitional Dark and Metallic classes, as shown in Fig. 3(d). For the image acquired on 26 January 2022, the Sentinel-2B true colour composite, oil spill classification, OSI, and oil slick spectral signature are shown in Figure 3.

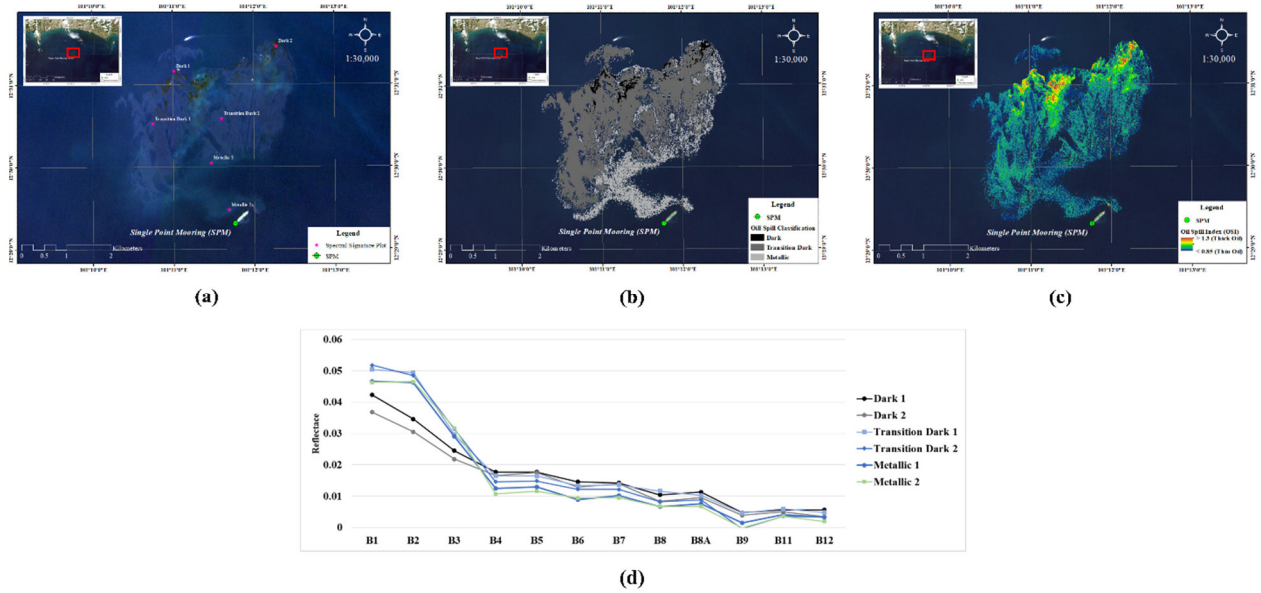

Figure 3. Comparison of results from Sentinel-2B MSI imagery on 26 January 2022 showing (a) Sentinel-2B MSI RGB (True Colour Composite: 432), (b) oil spill classification using K-mean clustering analysis, (c) OSI, and (d) Spectral signature on oil slick

3.1.2 Oil Spill on 27 January 2022

The oil slick detected from TerraSAR-X imagery on 27 January 2022 at 18:23 UTC+7 was found at a maximum distance of around 18 km from the SPM having moved towards the northeast and east. Based on the K-mean clustering analysis, the oil slick area was approximately 42.17 km^2 with more oil-spreading areas than the previous day. Based on Equation (2), the average DR value calculated for the oil slick area was 2.08 (±0.53 STD), with a calculated DR value range of 1.00–10.58 for the image. The VV backscattering (dB) analysis for a line profile is shown in Figure 4 (d). The results show a clear difference in intensity between clean seawater and the oil-slicked area, where the DR value can also indicate oil slick thickness variations and identify areas containing thicker oil in each area. The TerraSAR-X image from 27 January 2022, oil spill detection, DR variation, and line profile plot of intensity in dB across the oil slick are shown in Figure 4.

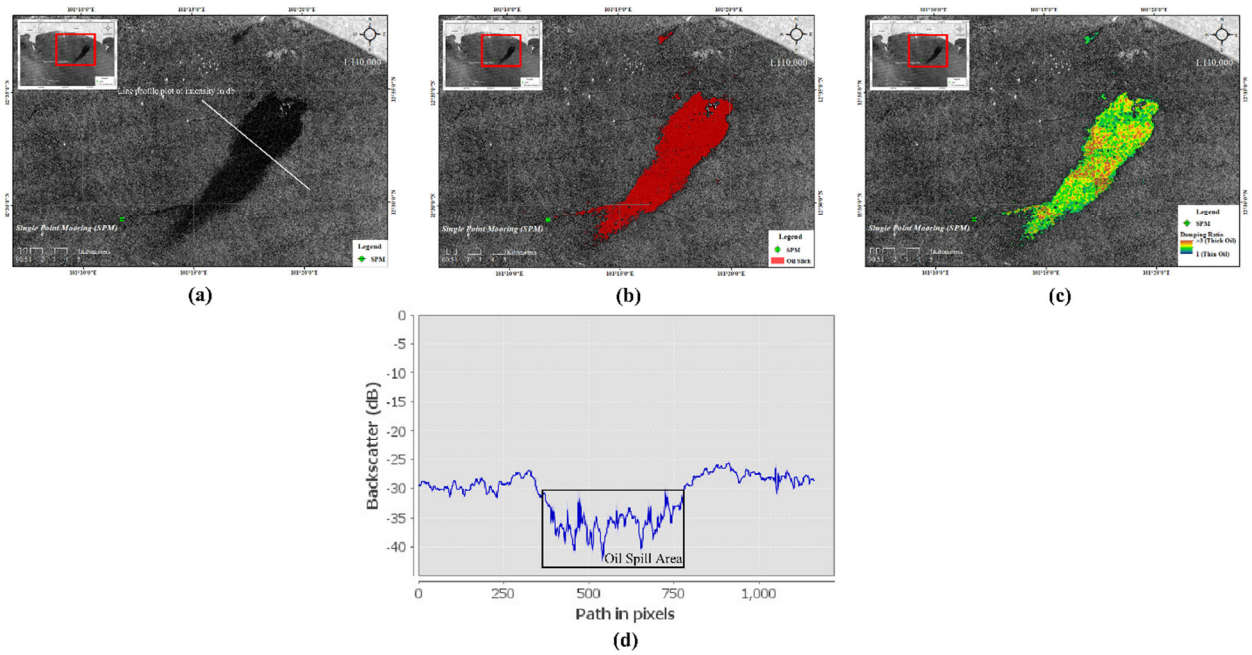

Figure 4. Results from TerraSAR-X1 imagery acquired on 27 January 2022, including (a) TerraSAR-X1 image, (b) oil spill classification using K-mean clustering analysis, (c) DR values, and (d) line profile plot of backscattering in dB

3.1.3 Oil Spill on 30 January 2022

The oil slick detected in ICEYE-X8 imagery from 30 January 2022 at 09:57 UTC+7 was found at a maximum distance of around 24 km from the SPM, indicating oil slick movement towards the northeast. At this time, the oil slick was located in both the sea and coastal area. The oil slick area determined by K-mean clustering was approximately 11.12 km^2. The average DR value for the oil slick area was 1.32 (±0.10 STD), and the image had a DR value range of 1.00–2.13. The VV backscattering values (dB) from a line across the oil slick are shown in Figure 5 (d). The results show that the DR value characterises oil slick thickness variations, with lower DR values recorded than on 27 January 2022, thus indicating a thin oil slick in this area. The ICEYE-X8 image from 30 January 2022, oil spill detection, DR variation, and line profile plot of backscattering intensity across the oil slick are shown in Figure 5.

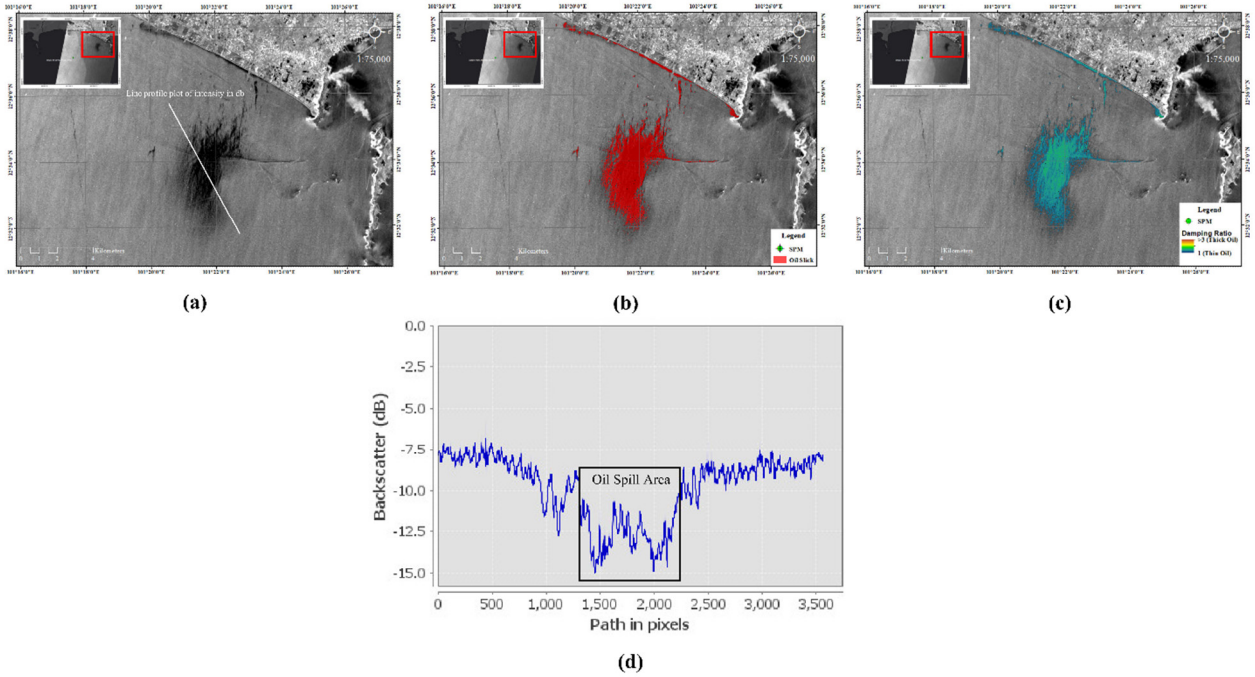

Figure 5. Results from ICEYE-X8 imagery acquired on 30 January 2022, including (a) ICEYE-X8 image, (b) oil spill classification using K-mean clustering analysis, (c) DR values, and (d) line profile plot of backscattering in dB

3.2 Evaluation of Oil Spill Thickness Classification

The oil spill detection and thickness classification results were evaluated by comparing them with Thaichote images acquired during the oil spill incident and other ancillary data such as ocean condition data and news reports from the area. The wind speed from Rayong station during the oil spill incident (26–30 January 2022) was an average of 2.19 m/s, with the strongest winds predominantly from the south and southwest. The surface current data indicate a predominant current direction towards the east and northeast with a speed of around 0.1–0.5 m/s. Overall, the identified speed and movement direction of the oil slick are consistent with the study of Polsomboon and Sriariyawat (2022) which simulated the oil slick's trajectory using the General NOAA Oil Modelling Environment (GNOME) model. The wind and surface current data in the present study are consistent with the movement of the oil spill, the spreading of the oil, the slick's natural weathering process over time, and the affected coastal areas detected from satellite images, as shown in Figure 6.

The results indicate that the OSI obtained from the Sentinel-2B image on 26 January 2022 successfully characterised the oil spill incident, allowing for effective spill classification and estimation of the oil thickness. These outcomes are consistent with the study of Rajendran et al. (2021a), which showed that OSI can be used to study the characteristics of oil spill absorption and discriminate spills as thick or thin oil. The results in this study were achieved by comparing the visible appearance of oil slicks with the oil code colour and relative thickness values defined by the NOAA's Emergency Response Division (NOAA, 2016). The DR results derived from the TerraSAR-X image on 27 January 2022 allowed the detection of the remaining oil spills and the identification of areas with varying oil thicknesses. The results are consistent with the Thaichote image taken on 28 January 2022, as shown in Figure 6 (b), in which predominantly metallic oil slicks are observed, with a reduced oil slick thickness compared to the first day of the incident. The DR values from the ICEYE X-band image on 30 January 2022 reveal the remaining oil slick as thin oil. The Thaichote image from 29 January 2022 corroborated these findings, indicating that some of the oil slicks had reached the shoreline by this date, consistent with field data and news reports in the area (Reuters, 2022). In the Thaichote image on 30 January 2022, no substantial oil slicks were observed, with only sheen layers indicative of a thin oil film. Overall, these results are consistent with previous studies (Minchew et al., 2012; Garcia Pineda et al., 2013; Jones and Holt, 2018; Garcia-Pineda et al., 2020), which show that the DR is a valuable index for detecting emulsions, separating thin from thick oil, and determining the oil:water volumetric fraction.

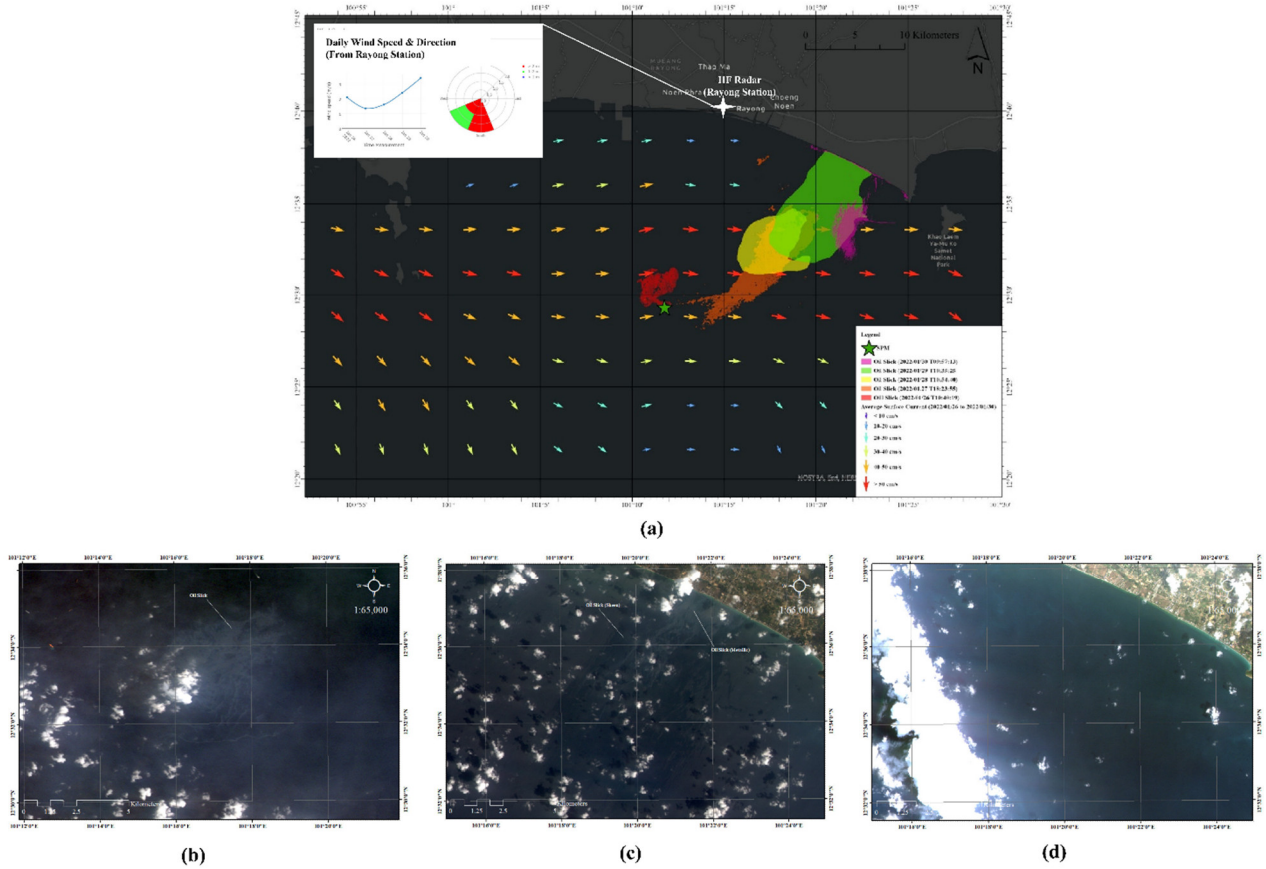

Figure 6. Evaluation of oil spill during the studied incident. (a) Oil spill extent during the oil spill incident (26–30 January 2022) with wind and surface current data; Thaichote imagery on (b) 28 January 2022, (c) 29 January 2022, and (d) 30 January 2022

4. CONCLUSION

In this study, optical and microwave remote sensing were implemented to detect and classify the thickness of oil spills, including a case study of an oil spill incident at the SPM in the Gulf of Rayong on 25 January 2022. Sentinel-2B MSI imagery was employed to calculate the OSI based on optical remote sensing for oil spill detection and thickness classification. In addition, TerraSAR-X and ICEYE X-band images were used to calculate the DR for oil spill detection and thickness characterisation. The OSI obtained from the Sentinel-2B image on 26 January 2022 successfully captured the oil spill incident, allowing for effective classification and estimation of the oil thickness, which was achieved by using the oil code colour and relative thickness classes approach presented by the NOAA's Emergency Response Division. Subsequently, the movement of the oil spill and its natural weathering process over time resulted in some oil patches impacting coastal areas. The DR calculated from the TerraSAR-X image on 27 January 2022 and the ICEYE X-band image on 30 January 2022 allowed the detection of the remaining oil spills and the identification of areas characterised by varying oil thicknesses. These findings were corroborated by Thaichote imagery and field data, with no substantial oil slicks observed by 30 January 2022 and only sheen layers present, indicating a thin oil film. The results of this study indicate that optical and microwave remote sensing are reliable and effective tools for monitoring oil spills and determining oil thickness characteristics.

ACKNOWLEDGEMENT

This study was accomplished with the cooperation of the colleague and the relevant agencies. We also thank GISTDA for their financial and facilities support.

REFERENCES

Alabdouli, A.S.J, Kalathingal, M.S.H, Mirza, S.B., Ridouane, F.L., 2023. Effective Oil Spill Monitoring Approach over the Gulf of Oman by Using Advanced Machine Learning and Data Mining Tools. *Int J Swarm Evol Comput*, 12 (02), 1000301.

Brekke, C., Jones, C.E., 2020. *SAR oil spill imaging, interpretation and information retrieval techniques*. In: Iodice, Di Martino. Maritime Surveillance with Synthetic Aperture Radar. The Institution of Engineering and Technology, 227-267.

Buranapratheprat, A., 2008. Circulation on the Upper Gulf of Thailand: a review. *Burapha Science Journal*, 13(1), 75-83.

Chatziantoniou, A., Karagaitanakis, A., Bakopoulos, V., Papandroulakis, N., Topouzelis, K., 2021. Detection of Biogenic Oil Films near Aquaculture Sites Using Sentinel-1 and Sentinel-2 Satellite Images. Remote Sensing, 13(9), 1737. https://doi.org/10.3390/rs13091737.

Espeseth, M.M., Jones, C.E., Holt, B., Brekke, C., Skrunes, S., 2020. Oil-Spill-Response-Oriented Information Products Derived From a Rapid-Repeat Time Series of SAR Images. *IEEE Journal of Selected Topics in Applied Earth Observations and Remote Sensing*, 13, 3448 – 3461.

Fingas, M. 2013. The Basics of Oil Spill Cleanup, 3rd ed. CRC Press, 286 pp.

Garcia-Pineda, O., MacDonald, I., Hu, C., Svejkovsky, J., Hess, M., Dukhovskoy, D., Moorey, S., 2013. Detection of oating oil anomalies from the Deepwater Horizon oil spill with synthetic aperture radar. Oceanography 26 (2), 124–137. https://doi.org/10.5670/oceanog.2013.38.

Garcia-Pineda, O., Staples, G., Jones, C.E., Hu C., Holt, B., Kourafalou, V., Graettinger, G., DiPinto, L., Ramirez, E., Streett, D., Cho, J., Swayze, G.A., Sun, S., Garcia, D., Haces-Garcia, F., 2020. Classification of oil spill by thicknesses using multiple remote sensors. *Remote Sensing of Environment,* 236, 111421.

Ingviya, T., Intawong, C., Abubaker, S., Stricklandet, S.T., 2020. Exposure Assessment of Rayong Oil Spill Cleanup Workers. Expo Health 12, 617–628. https://doi.org/10.1007/s12403-019-00320-0

Jones, C.E., Holt, B., 2018. Experimental L-band airborne SAR for oil spill response at sea and in coastal waters. Sensors 18 (2), 641. https://doi.org/10.3390/s18020641.

Laffon, B., Pasaro, E., Valdiglesias, V., 2016. Effects of exposure to oil spills on human health: updated review. *J Toxicol Environ Health B Crit Rev* 19(3–4), 105–128. https://doi.org/10.1080/10937 404.2016.1168730

Minchew, B., Jones, C.E., Holt, B., 2012. Polarimetric analysis of backscatter from the deepwater Horizon oil spill using L-band synthetic aperture radar. IEEE Trans. Geosci. Remote Sens. 50 (10), 3812–3830. https://doi.org/10.1109/TGRS.2012.

NOAA, 2016. Open Water Oil Identification Job Aid (NOAA-CODE) for Aerial Observation. With Standardized Oil Slick Appearance and Structure Nomenclature and Codes. U.S. Department of Commerce, National Oceanic and Atmospheric Administration, Office of Response and Restoration, Emergency Response Division, Seattle, Washington USA.

Polsomboon, P., Sriariyawat, A., 2017. Effect of Monsoon Wind to Current in East Coast of the Gulf of Thailand. Internet Journal of Society for Social Management Systems, 11 (1), 17-2604.

Polsomboon, P., Sriariyawat, A., 2022. Oil Spills simulation in Rayong coastal area : case study oil spill on 26 January 2022. In: *The 27th National Convention on Civil Engineering*, August 24-26, 2022, Chiang Rai, Thailand.

Rajendran, S., Vethamony, P., Sadooni, F.N., Al Saad, H., Jassim, A., Al-Kuwari, G.A.S, Al-Khayat, J.A., Govil, H., Sobhi Nasir, S., 2021a. Sentinel-2 image transformation methods for mapping oil spill - A case study with Wakashio oil spill in the Indian Ocean, off Mauritius. *MethodsX*, 101327.

Rajendran. S, Vethamony. P, Sadooni F.N, Hamad Al Saad, Jassim A. Al-Kuwari, G.A.S, Al-Khayat, J.A., Seegobin, V.O., Govil, H., Sobhi Nasir, S., 2021b. Detection of Wakashio oil spill off Mauritius using Sentinel-1 and 2 data: Capability of sensors, image transformation methods and mapping. *Environmental Pollution*, 274, 116618.

Reuters, 2022. Thai beach declared disaster area after oil spill. Source: https://www.reuters.com/world/asia-pacific/thai-beach-declared-disaster-area-after-oil-spill-2022-01-29/.

Saengtabtim, K., Laosunthara, A., Tang, J., Leelawat, N., 2023. The 2022 Rayong Oil Spill Crisis in Thailand: An Identification for Reliability and Nearly-Real Time Data using Twitter. 2023 Third International Symposium on Instrumentation, Control, Artificial Intelligence, and Robotics (ICA-SYMP), Bangkok, Thailand, 2023, 118-122. https://doi.org/10.1109/ICA-SYMP56348.2023.10044941.

Sergievskaya, I., Ermakov, S., Lazareva, T., Guo, J., 2019. Damping of surface waves due to crude oil/oil emulsion films on water. *Mar. Pollut. Bull.,* 146, 206–214.

Skrunes, S., Brekke, C., Espeseth, M.M., 2017. Assessment of the RISAT-1 FRS-2 mode for oil spill observation," *in Proc. IEEE Int. Geo. Remote*
Sens. Symp., 1024–1027.

Skrunes, S., Johansson, M.A., Brekke, C., 2019. Synthetic Aperture Radar Remote Sensing of Operational Platform Produced Water Releases. *remote sensing,* 11, 2882.